Check for updates

Methylcellulose/agarose hydrogel loaded with short electrospun PLLA/laminin fibers as an injectable scaffold for tissue engineering/3D cell culture model for tumour therapies†

Beata Niemczyk-Soczynska, [ID] [a] Dorota Kolbuk, [ID] [a] Grzegorz Mikulowski,[a] Iwona A. Ciechomska[b] and Pawel Sajkiewicz [ID] *[a]

This research aimed at designing and fabricating a smart thermosensitive injectable methylcellulose/agarose hydrogel system loaded with short electrospun bioactive PLLA/laminin fibers as a scaffold for tissue engineering applications or 3D cell culture models. Considering ECM-mimicking morphology and chemical composition, such a scaffold is capable of ensuring a hospitable environment for cell adhesion, proliferation, and differentiation. Its viscoelastic properties are beneficial from the practical perspective of minimally invasive materials that are introduced to the body *via* injection. Viscosity studies showed the shear-thinning character of MC/AGR hydrogels enabling the potential injection ability of highly viscous materials. Injectability tests showed that by tuning the injection rate, even a high amount of short fibers loaded inside of hydrogel could be efficiently injected into the tissue. Biological studies showed the non-toxic character of composite material with excellent viability, attachment, spreading, and proliferation of fibroblasts and glioma cells. These findings indicate that MC/AGR hydrogel loaded with short PLLA/laminin fibers is a promising biomaterial for both tissue engineering applications and 3D tumor culture models.

1. Introduction

Diseases and accidents leading to the injury of the central nervous system (CNS), *i.e.*, the brain and spinal cord, are extremely challenging from the perspective of medicine and tissue engineering. The reason for that is progressive, irreversible neuron degeneration, and lack of particular targeted therapy.[1,2] Injuries and diseases of the CNS have always been a serious global socioeconomic problem. According to global statistics, spinal cord injury (SCI) affects over 500 000 people every year according to Global incidence data,[3] while traumatic brain injury is experienced by 27 000 000 people every year.[4] In 2016, there were 330 000 CNS cancer cases, particularly brain tumors.[5] Since currently brain tumors lead to 190 000 deaths per year,[6] there is huge demand to find therapies that allow a better understanding of tumour cell behavior and, subsequently, implementation of targeted therapy.

Current clinical TBI strategies focus on therapeutic agents (such as drugs, cells or growth factors) delivery, scaffold

implantation, or combining both of those approaches.[7] Although therapeutic agent delivery alone seems to be the perfect strategy, only their low concentrations actually reach the injured area of the CNS. In addition, growth factors might rapidly degrade after being introduced into the body, while cell transplantation shows the possibility of cell migration to the other CNS areas resulting in abnormal growth of the tissue or performing poor viability due to an unfavorable environment for cell growth.[7,8] Increasing doses of therapeutic agents to trigger the desired therapeutic effect could lead to systemic toxicity.[9] To overcome this problem, invasive therapeutics delivery is widely used. Such a method allows the delivery of high doses of therapeutics into injured areas and avoids exposure of the surrounding tissues to the applied drug. However, such treatment also disrupts the blood–brain barrier (BBB) and is conducted *via* complex surgeries.[10] This is especially common for brain tumor therapies, where chemotherapeutics are delivered directly to the tumor and at the same time, do not enter the systemic circulation. However, complex brain or spinal cord surgeries carry a huge danger of after-surgery complications such as subsequent neuronal damage or inflammations.[7]

Most of the current clinical approaches focus on drug/cell delivery only, but not on providing ECM-mimicking nontoxic microenvironment restoring neurons' main functions. Consequently, the currently available clinical therapies, including

[a]Institute of Fundamental Technological Research, Polish Academy of Sciences, Pawinskiego 5b St., 02-106 Warsaw, Poland. E-mail: psajk@ippt.pan.pl

[b]Nencki Institute of Experimental Biology PAS, 3 Pasteur Street, 02-093 Warsaw, Poland

surgeries and less invasive treatments, focus mostly on post-trauma relief but do not provide real prolonged therapeutic effects or effective regeneration of injured CNS.[3] These limitations could be overcome by implementing the scaffold in the injured areas that mimic the natural ECM of CNS providing excellent conditions for cell regeneration.[11] Additionally, CNS mimicking microenvironment could be useful as a 3D cell culture model to investigate and understand brain tumors, *i.e.*, cellular morphology, phenotype, gene expression pattern, mechanism of spreading, tumor-immune cell interactions, and drug resistance.[12]

A new approach of natural minimally invasive and "smart" biomaterials such as injectable hydrogels loaded with nanoparticles or nanofibers (*e.g.*, ref. 13 and 14) are in the area of recent interest in tissue engineering. In this field, injectable *in situ* crosslinked hydrogels offer many advantages such as good biocompatibility and processability. The injectability of such materials determines their non-invasive and fast introduction into the lesion, which allows for avoiding long and complex surgeries.[15] Hydrogels form 3D structures that characterize large amounts of water in a polymeric network mimicking the brain extracellular matrix (ECM), which stimulates stem cell adhesion, proliferation, and differentiation for neural tissue engineering. Such mimicry makes hydrogels an important supporting factor that provides better cell integrity with the material.[16,17] In some stimuli-responsive types of hydrogel, external stimulation, like pH, or temperature change provoke its crosslinking. Nevertheless, hydrogels usually perform poor mechanical properties and lack fibrous structure providing adequate support for cell activity.[18,19] For instance, Thonhoff *et al.*[20] tested commercially available hydrogels of Matrigel and PuraMatrix with fetal human neural stem cells (hNSCs) regarding cytotoxicity and stem cell support ability and differentiation. The studies showed that tested hydrogels supported cells insufficiently resulting in reduced survival of hNSCs and poor migration capabilities within the injured cavity.

According to Ucar *et al.*[7] combination of appropriate natural and synthetic biomaterials might overcome all of these problems by providing a hospitable environment that mimics native ECM, for tissue regeneration. Such an environment should provide biocompatibility, adequate support for cells, and, consequently adequate mechanical properties, *i.e.*, 1–10 kPa for the brain,[21] and 0.52–1.88 MPa for the spinal cord.[22] Besides those properties, a perfect material should mimic ECM biochemically, to provide good cell-material (*i.e.*, cell-ECM proteins/proteoglycans interactions) and cell–cell interactions. This has been shown to play a crucial role in cell fate.[23,24] In this respect, the incorporation of native ECM components such as peptide sequences that interact with cell membrane integrins Ile-Lys-Val-Ala-Val (IKVAV) or growth factors (neurotrophic growth factors (NGFs)).[25,26]

Most of the current research dedicated to neural tissue engineering focuses on hydrogels loaded with nanoparticles, which are considered safe and effective in delivering cells or drugs into the injured area.[27] One example is thermoreversible gelation polymer (TGP) loaded with poly(lactic-*co*-glycolic acid) (PLGA) microspheres for rats' glioma treatment.[28] However,

similarly to drug delivery systems, too few nanoparticles can be absorbed by macrophages immediately after injection into the body;[27] thus, most of these approaches seem not applicable as a supportive structure for neural cells.

Currently, cellulose-based materials and hydrogels strengthened with short nanofibers are becoming increasingly popular in tissue engineering, and medicine but also 3D cell culture models, *i.e.*, a well-defined platform that maintains cell viability and replicates native cellular environments similar to those found in tissues. This technology provides mechanical, biochemical, morphological, and physiological guidance on the properties of tumor cells in a 3D environment. One of the examples of using cellulose-based materials is hydrogel consisting of collagen/nanocellulose nanofibers as a 3D model for developing a therapy against pancreatic ductal adenocarcinoma (PDAC).[29]

In this work, we propose a thermosensitive injectable hydrogel system loaded with short electrospun biologically active fibers that have been studied as a potential scaffold for the central nervous system (CNS) tissue engineering or 3D glioblastoma culture model. The base component of the proposed hydrogel systems is the cellulose derivative of methylcellulose (MC) approved by the Food and Drug Administration (FDA). The MC alone undergoes thermal reversible crosslinking as an effect of the temperature increase near 37 °C. The crosslinking mechanism of MC is a result of a unique type of dehydration based on "water cages" destruction, and subsequent 3D fibril network formation, which was thoroughly discussed in our previous studies.[30–32] Another hydrogel component is agarose (AGR), which strengthens the hydrogel mechanically and fulfils an important function of the MC crosslinking rate accelerator by faster dehydration of water cages of MC.[32] The MC/AGR hydrogel properties were additionally enriched by introducing the short electrospun fibers. Short electrospun fibers are especially valuable while designing hydrogel composite systems. Similarly to the fibrous mats such fibers strengthen and improve hydrogel mechanically, and after proper biological functionalization also biochemically. Contrary to fibrous mat, short fibers could be easily dispersed in the liquid media, *e.g.* hydrogel solution. Additionally, short fibers provide ECM mimicry and injection ability of whole composite material, which in the case of tissue engineering allows avoiding long-term complex surgeries. The such minimally invasive solution increases potential patients' comfort and faster convalescence.[33,34]

Electrospun-oriented PLLA fibers are widely used as scaffolds for neural tissue regeneration, mainly due to their biocompatibility, controlled degradation, and mechanical properties similar to neural tissue. The fibrous structure effectively supports the regeneration of neurons in both *in vitro* and *in vivo* conditions.[35,36] PLLA was also selected due to its appropriate stiffness and brittleness necessary for further fragmentation using ultrasonication. Nevertheless, most synthetic electrospun fibers are biochemically inert and hydrophobic, which also concerns PLLA fibers. Consequently, electrospun PLLA fibers needed adequate modifications. The first one, described in detail in our previous studies,[33] is fragmentation using ultrasonication which is to ensure the appropriate size of fibers to maintain the possibility of hydrogel injection. The second one, described in this article, was PLLA fiber modification by protein immobilization using the physical

adsorption method; such an approach overcame fibers' biological inertia. Considering CNS tissue engineering requirements and our goal to provide an appropriate microenvironment by our hydrogel system, laminin was the protein that was chosen. Laminin is one of the key ECM components that provides an effective site of IKVAV for neuronal cell adhesion and increased hydrophilicity of the short PLLA fibers. This protein is essential, especially for nerve regeneration – it effectively binds Schwann cells, and regeneration of axons takes place only in the laminin presence.[35,37]

Although MC/AGR/PLLA/fibronectin hydrogel system for brain therapy was studied previously by Rivet *et al.*,[18] we present new chemical composition of MC/AGR/PLLA/laminin that was not previously described in the literature. Additionally different materials characteristic was conducted in our studies than this described in ref. 18, which could provide new insight in designing similar approaches.

The objective of these studies was to design and fabricate a thermosensitive injectable hydrogel system that provides a hospitable environment for cell regeneration. Such an approach might serve as scaffold cell regeneration as well as a 3D cell culture model that mimics the spatial organization of neural tumors to develop new anti-cancer therapies. In this respect, MC/AGR hydrogel loaded with short electrospun PLLA/laminin fibers was designed and investigated in terms of viscosity, injectability, morphology, and the biological properties studied in direct contact with L929 fibroblasts as well as LN18 and WG4 glioma cells. Such characteristics allowed us to evaluate the potential and significance of the hydrogel system for neural tissue engineering applications and as a 3D tumor cell culture model.

2. Experimental

2.1. Preparation of MC/AGR solution

The MC and AGR powder were sterilized *via* UV for 30 min. In order to provide equal sterilization the powders were gently shaken every 10 min. The 3 and 5 wt% MC (METHOCEL A15LV, Sigma Aldrich) was added to the 3 and 3.5 wt% AGR (SeaPrepR, Lonza) aqueous solutions respectively. The powder MC and AGR were dissolved in phosphate-buffered saline (PBS, Life Technologies) separately and stirred overnight. Then, the AGR solution was mixed with the MC solution and left to stir overnight to provide a homogeneous mixture of both solutions.

The thermal physical crosslinking of MC/AGR took place under temperature increase at *ca.* 37 °C as described in our previous publications.[31,32]

2.2. MC/AGR degradation

The 3MC/3AGR and 5MC/3.5AGR hydrogel samples for degradation tests were soaked in PBS at 37 °C to mimic the physiological environment for 3 weeks. The specific procedure was conducted as follows:

(1) Each 2 ml micro-centrifuge tube was weighed before and after addition of 500 µl of hydrogels (21 samples for each group, w2-w1 was assigned as wet weight ww). The hydrogels were

stored overnight at 37 °C in incubator to provide thermal physical gelation.

(2) 500 µl of PBS previously stored at 37 °C was added to the tube with hydrogel samples. The addition of heated PBS was in order to avoid hydrogel degelation.

(3) All of the samples were marked and put into an incubator at 37 °C.

(4) The PBS was changed every 3 days.

(5) At 1, 2, 4, 6, 8, 12, 18 day (*t*), three samples of each group were taken out, the PBS was removed, and samples were dried in a vacuum dryer (MEMMERT VO) at 50 mBar for 24 h at room temperature. Dry weight (wd(*t*)) of each sample was weighed.

In respect to the samples weight from the 1st day, dry to wet weight ratio of 3MC/3AGR and 5MC/3.5AGR were calculated (wd(1)/ww(1)). According to this the theoretical initial dry weight at *t* day was calculated according the following equation:

$$\mathrm{wd}(t)^* = \mathrm{ww}(t) \times \mathrm{wd}(1)/\mathrm{ww}(1)$$

Degradation at *t* day was determined from the following equation:

$$\mathrm{Degradation}\ (t) = \frac{\mathrm{wd}(t)^* - \mathrm{wd}(t)}{\mathrm{wd}(t)^*} \times 100\%$$

2.3. Preparation of short PLLA/laminin electrospun fibers

PLLA fibers with oriented morphology (PURASORB PL 49, Purac, Netherlands) were electrospun and subsequently fragmented using ultrasonication as previously described.[33] Their average length after ultrasonication was in the range of 40–60 µm. The PLLA mats and short fibers were sterilized using a UV light for 30 min, and then with 70% ethanol and left overnight to evaporate the residuals of ethanol. The SEM images of PLLA fibers before and after ethanol treatment were included in ESI (Fig. A†). Ethanol caused slight fibers relaxation, but the fiber morphology changes were not significant. After that, laminin was immobilized to the PLLA mats and short fibers by physical adsorption. Fiber samples without immobilized protein served as a reference. The 1 mg of laminin from Engelbreth–Holm–Swarm murine sarcoma basement membrane (Sigma Aldrich) was dissolved in PBS to obtain the protein concentration of 41 µg ml^{-1}. The solution was vortexed delicately for 2 h. The PLLA fiber mat and short fibers were immersed in laminin solutions for 24 h at 4 °C. All of the samples were washed 3 times with demineralized water for 8 h to remove non-adherent proteins.

2.4. Preparation of short fibers/hydrogel system

The PLLA and PLLA/laminin short fibers were added to the MC/AGR hydrogels at 2.5 mg ml^{-1} and 5 mg ml^{-1} and stirred on a magnetic stirrer overnight.

2.5. Fiber characterization

2.5.1 Water contact angle (WCA). The WCA measurements of electrospun mats were carried out to evaluate the changes in

the PLLA fiber's surface wettability before and after the physical adsorption of laminin. Additionally, some PLLA samples were selected and treated with 70% ethanol to decrease the surface tension of fibers and increase the amount of immobilized protein.[38] After ethanol evaporation, PLLA fibers were modified with laminin.

All of the measurements were conducted with the use of Data Physics OCA 15EC (Germany) using the sessile drop method. A 2 μl water drop was dispensed onto the surface of the fibers. The surface contact angles were measured at 1 and 3 s.

2.5.2 Bicinchoninic acid assay (BCA) assay. Total protein adsorption was assigned by using the BCA assay (Sigma Aldrich). BCA protocol assumes the formation of purple-coloured products obtained in the chelation reaction of two bicinchoninic acid molecules with Cu^+. The BCA working reagent preparation assumed mixing 50 parts of BCA reagent A, 50 parts of BCA reagent B, and 1 part of BCA C. Protein adsorption was determined for the previously ethanol-treated, rinsed with water, and dried PLLA electrospun mats and short fibers. The laminin solutions at concentrations of 0, 0.5, 5, 10, 15, 20, 25, and 30 μg ml^{-1} served as a standard curve.

After being weighed, mats and short fibers were placed in a 24-well plate, soaked in 200 μl of PBS, and incubated at 37 °C for 2 h. After that, 200 ml of BCA solution was added to each fibrous sample, and laminin dilutions for a standard curve, and were gently shaken at 37 °C for 2 h.

The absorbance at 562 nm was determined by a microplate spectrophotometer (Fluoroskan Ascent, Thermo Scientific). From obtained absorbance, the average absorbance values of blank samples were subtracted, and subsequently, normalized values were plotted as a function of mass concentration (g L^{-1}).

2.6. Hydrogel system/short fibers characterization

2.6.1 Viscosity. The viscosities of 3MC/3AGR and 5MC/3.5AGR hydrogel without fibers and filled with 2.5 mg ml^{-1} and 5 mg ml^{-1} of PLLA PL 49 short fibers were measured *via* HADV-III Ultra viscometer equipped with a cone/plate geometry (CP-52 (cone angle 3°)). The measurements were carried out at a constant temperature of 22 °C and 37 °C, and various constant shear rates of 50, 100, 200, 300, 400, 500, and 500 s^{-1}. Very low and high viscosities beyond the measurement possibilities were extrapolated numerically using the Carreau regression model which fit well with the experimental results.[39]

2.6.2 Injectability test. Evaluation of MC/AGR and MC/AGR/PLLA injectability was carried out *via* a servo hydraulic loading actuator (MTS Systems GmbH). The system was electronically controlled based on a displacement LVDT sensor in order to perform an accurate expansion velocity. The stand was interchangeably equipped with two various Interface load cells of 1500ASK-1000N and 1500ASK-125N of two measuring ranges: max. 1000 N and max. 125 N (Interface, Inc., Scottsdale, Arizona, USA). The 1 ml of each solution was loaded into the 1 ml glass syringe (FORTUNA OPTIMA Ganzglasspritze, Poulten Graf GmbH, Germany) coupled with a 23 gauge needle (d = 0.34 mm). The syringe was placed in a special holder, where the tip of the piston was in contact with the dynamometer, and the syringe was

pointing downwards. The solutions were injected into previously heated and thermally crosslinked 2.5 wt% MC hydrogel, having a shear modulus that corresponds to the native human spinal cord.[31] To keep 2.5 wt% MC in crosslinked form as well as provide conditions that fairly mimic the *in vivo* conditions, the hydrogel solution was heated to 37 °C during all injectability tests.

The 1 ml of solutions were injected with two different flow rates of 1 ml min^{-1} and 0.125 ml min^{-1}. During an experiment of hydrogel injection, the injection force was registered. According to many literature reports, *i.e.* Kim *et al.*[40] the force of 50 N is considered to be the maximum value above which a manual injection is impossible. To evaluate the maximum force needed to perform the injection, the highest registered values were taken, averaged from the three measurements, and subsequently determined as the average maximum injectability force for each sample. The measurements were acquired *via* an individually prepared electronic code that was based on the MTS Systems testing environment.

2.6.3 Hydrogel system/short fibers morphology. The morphology of hydrogel loaded with short electrospun nano-fibers was investigated using a Scanning Electron Microscope (SEM) (JEOL JSM-6390LV, Japan). Before imaging samples were placed into the freezer at −70 °C overnight. Then frozen samples were freeze-dried in a vacuum freeze dryer to remove water residuals. All of the freeze-dried samples were sputtered with 8 nm of gold. The acceleration voltage was 7 kV.

2.6.4 Biological tests. Based on the results of our previous studies, *i.e.*,[32] a hydrogel system of 5MC/3.5AGR was selected due to its good mechanical and biological properties. For biological studies, the following samples were studied: a pure 5MC/3.5AGR hydrogel, 5MC/3.5AGR with the addition of laminin (5MC/3.5AGR/L), 5MC/3.5AGR modified with 2.5 mg ml^{-1} short PLLA fibers (5MC/3.5AGR/F), 5MC/3.5AGR with the addition of laminin and modified with 2.5 mg ml^{-1} short PLLA fibers (5MC/3.5AGR/L/F) and 5MC/3.5AGR with the addition of laminin and modified with 2.5 mg ml^{-1} short PLLA/laminin fibers (5MC/3.5AGR/L/F/L).

Samples preparation: MC and AGR powder were sterilized with UV light for 30 min. While sterilizing, the powder was gently shaken every 10 min to provide homogenous sterilization. After that, MC and AGR powder was dissolved in sterile PBS. The choice of PBS as a solvent prevents hyperosmotic stress. For 3MC/3AGR/L, 5MC/3.5AGR/L, 3MC/3AGR/L/F/L, and 5MC/3.5AGR/L/F/L samples additionally 1mg of laminin was added to the solution.

Simultaneously, short electrospun fibers were sterilized with UV light for 30 min, then sterilized with 70 wt% ethanol and left under the hood for ethanol evaporation. After that sterile laminin was introduced to the fibers as reported in Section 2.4.2.

Then sterile hydrogel solutions and fibers were mixed and left overnight for stirring. The homogenous hydrogel solutions were stored for 72 h in the incubator at 37 °C to provide thermal crosslinking of the MC/AGR system as was previously reported.[32]

2.6.4.1 Evaluation of biocompatibility on mouse fibroblasts. Fibroblasts culture: biocompatibility tests were carried out with the use of the L929 line of fibroblasts (Sigma Aldrich). Cells were

cultured in 75 cm^2 flasks containing a medium prepared of High Glucose Dulbecco's Modified Eagle's Medium (DMEM), 10% fetal bovine serum (FBS), and 1% antibiotics. Cells were incubated in a 5% CO$_2$ environment at a constant temperature of 37 °C. Harvesting of the cells took place in 70–80% confluent flasks. In the first step cells in PBS. After that step, 5 ml of 0.05% of trypsin solution was added to the cells and placed in the incubator for a few minutes. Then the flask was tapped delicately in order to detach the cells. After obtaining harvested cells, 10 ml of culture medium was added and centrifuged. The centrifugation was carried out at an ambient temperature. The pellet was resuspended with a culture medium to obtain the required cell density.

Biocompatibility evaluation: to determine the cellular response to the prepared set of hydrogels loaded with short fibers, a series of different studies were performed including cytotoxicity on hydrogel extracts as well as cellular morphology evaluation in direct contact.

Extracts for *in vitro* tests were determined from 5 samples of each hydrogel type (100 µl) placed in a 48-well plate according procedure reported before.[41] Briefly, samples were immersed in 300 µl of culture medium per well, kept at 37 °C, and gently stirred for 24 h. For reference, along wells with samples, 5 wells without hydrogel were filled with the medium as well. At the same time L929 cell suspension was seeded into another 48-well plate in the same amount of wells as sample extracts plus control with density 2×10^4 cells per well and put in an incubator for 24 h. After that time the culture medium from cell-seeded wells was replaced with material extracts and the plate was placed in the incubator for another 24 h contact with materials.

In the next step, extracts were removed, and each well was filled with 180 ml of PBS and 20 ml of Presto Blue reagent. After this step, the plate was returned to the incubator for 60 min. This step was completed, and 100 ml from each well was transferred to the 96-well plate. The fluorescence read with excitation/emission 530/620 nm filters was measured with the use of 530/620 nm excitation/emission wavelength by Fluorescent Accent FL Thermo Fisher Scientific. The results were compared with the Presto Blue fluorescence of blank samples, which did not show metabolic activity, and the control (Tissue Culture Plate TCP), which showed 100% of metabolic activity.

Fibroblast morphology in contact with hydrogels was analyzed with microscopy. L929 cells were seeded on cross-linked hydrogels with the density of 5×10^4 per well in 250 ml of the medium in a 24-well plate. Before analysis, seeded cells were stained with the CellTrace™ Yellow Cell Proliferation Kit (Thermo Fisher Scientific). Briefly, 3 mg of CellTrace dye-labelled 1×10^6 cells, and the staining was carried out for 20 min. After 3 days, samples were observed under fluorescence microscopy (Leica AM TIRF MC).

2.6.4.2 Evaluation of morphology of glioma cells. Glioma cells culture. Human malignant LN18 glioma cells were obtained from American type culture collection and were cultured in Dulbecco's-modified Eagles' medium (DMEM) supplemented with 10% fetal bovine serum (FBS; Gibco, Invitrogen) and antibiotics: 100 ml^{-1} penicillin and 100 µg ml^{-1} streptomycin

(Gibco, Invitrogen) in a humidified atmosphere of CO$_2$/air (5%/95%) at 37 °C (Heraeus, Hanau). Cell lines were authenticated using multiplex cell authentication by Multiplexion in Heidelberg, Germany.

Patient-derived glioma cell culture WG4 (GBM WHO grade 4) was developed as previously described.[42] Cells were cultured in DMEM/Nutrient Mixture F-12, GlutaMAX™ medium (DMEM/F-12, GlutaMAX™) supplemented with 10% FBS (Gibco, Invitrogen) and antibiotics (100 U per ml penicillin, 100 µg ml^{-1} streptomycin) in a humidified atmosphere of CO$_2$/air (5%/95%) at 37 °C (Heraeus, Hanau).

For morphological analysis of glioma cells, LN18 or WG4 cells were seeded (5×10^4 or 3×10^4 per well, respectively) onto crosslinked hydrogels-coated 24-well plates in 300 ml of appropriate medium. Before seeding, glioma cells were stained with 5 µM CellTrace™ Yellow dye for 20 min according to the manufacturer's instructions (CellTrace TM Cell Proliferation Kit, Thermo Fisher Scientific). The changes in cell morphology were monitored at various times by fluorescence microscopy (OLYMPUS IX70) using excitation at 530–550 nm.

WG4 cell morphology in contact with hydrogels in higher magnification was analyzed with fluorescence microscopy. Similar to the above-described methodology, WG4 cells were stained with the CellTrace™ Yellow Cell Proliferation Kit (Thermo Fisher Scientific) and seeded on crosslinked hydrogels. After 1 and 3 days, samples were observed under fluorescence microscopy (Leica AM TIRF MC) in transmitted light axis brightfield mode (TL-BF) and fluorescence mode to show cellular-substrates integration.

2.6.4.3 Statistics. The one-way ANOVA method was used to evaluate the statistical significance between the wettability of unmodified PLLA fibers, PLLA modified with laminin, PLLA modified with EtOH, and subsequently with laminin; the amount of immobilized laminin to the electrospun, fragmented, and EtOH-modified PLLA fibers. Additionally, the same statistic was used to evaluate the statistical significance between the forces needed to inject hydrogel systems and hydrogel systems loaded with nanofibers; and biological studies. A Tukey's test of all groups evaluated the statistical significance between individuals. The statistical analyses were conducted for $p < 0.05$ using GraphPad Prism 9.4.1 Software. The p below 0.05 was considered to be significant statistically, where $0.05 > p > 0.01$ is assigned as "*", $0.01 > p > 0.001$ is assigned as "**", $p < 0.001$ is assigned as "***", while $p < 0.0001$ is assigned as "****".

The WCA, BCA, viscosity, injectability, and cytotoxicity data are shown as mean $\pm$ SD ($n = 3$).

3. Results

3.1. MC/AGR degradation

The degradation rate of MC/AGR showed sustained degradation of both 3MC/3AGR and 5MC/3.5AGR over 12 days. The full materials' degradation occurred after 18 days. The 5MC/3.5AGR resulted in slightly slower degradation than 3MC/3AGR during 12 days of degradation studies (Fig. 1).
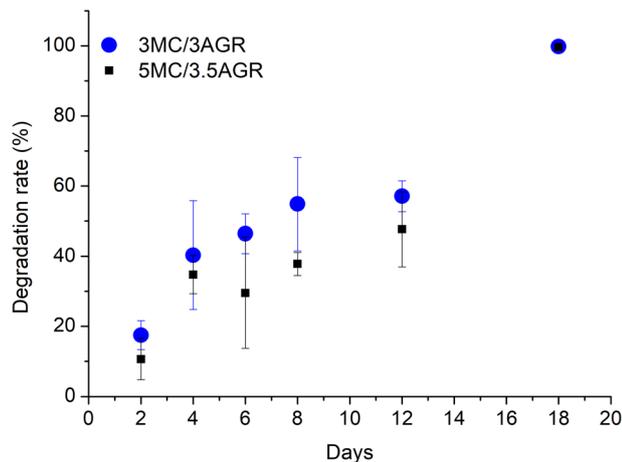
Fig. 1 Degradation of 3MC/3AGR and 5MC/3.5MC for 3 weeks at 37 °C.

3.2. Fiber characterization

3.2.1 WCA. The results of WCA measurements before and after laminin incorporation into the fibers are shown in Fig. 2. Additionally, some of the PLLA/laminin samples were previously treated with EtOH to decrease the surface tension of the fiber mat. The contact angles for all samples were in the range of 98–125 °. As predicted, the short fiber samples modified with laminin and previously modified with EtOH and laminin showed a slight decrease in contact angle compared to the non-treated samples (Fig. 2).

3.2.2 BCA. Surface modification with proteins *via* physical adsorption involves such interactions as electrostatic, hydrogen, hydrophobic, and van der Waals, which allows good biomolecule adhesion to the fibers surface.[43,44] Laminin was selected to determine its adhesion ability to electrospun mats as well as short fibers made of PLLA. Since there are many reports of qualitative studies of laminin-PLLA relations using X-ray photoelectron spectrometry (XPS) (*e.g.* ref. 35, 45 and 46), our studies were focused on quantification of laminin coupled onto fibers *via* BCA assay (Fig. 3). The two parameters that were considered to improve laminin adsorption were taken into account. One of them was a higher area of short fibers, while another was the additional treatment of PLLA fibers with EtOH before they were adsorbed with laminin.

The BCA assay indicated that both factors – fibers fragmentation and EtOH treatment lead to an increase in the amount of adsorbed laminin on the fibers surface, resulting in the highest adsorption for short fibers treated with EtOH (Fig. 3).

3.3. Short fibers/hydrogel system characterization

3.3.1 Viscosity. The viscosity was determined for 3MC/3AGR and 5MC/3.5AGR at different shear rates at room and physiological temperatures. The viscosity measurements as a function of shear rates indicate non-Newtonian shear-thinning characters of investigated hydrogels (Fig. 4). The Carreau model, commonly used to describe shear-thinning fluids [*e.g.* ref. 48], was well fitted to our experimental data, with R^2 >
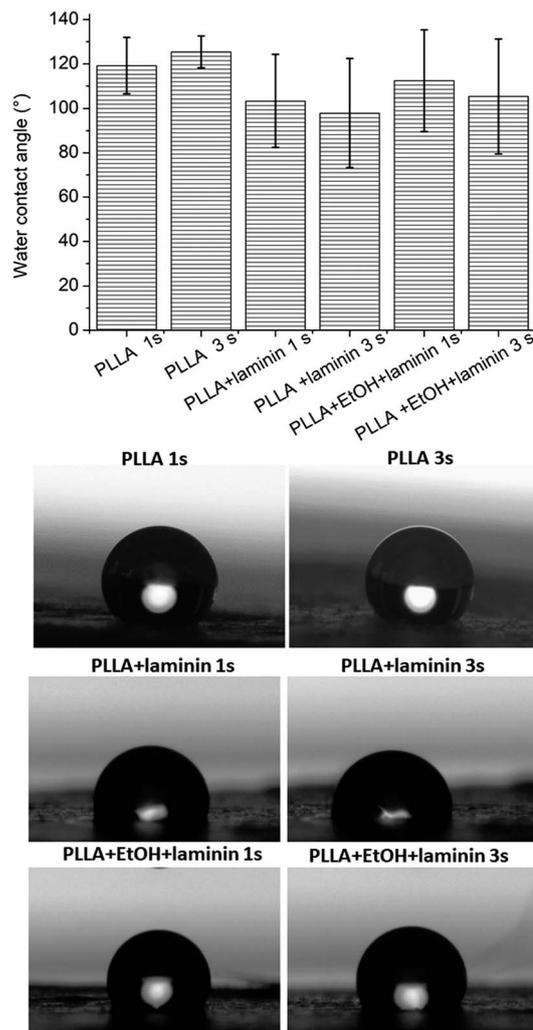

Fig. 2 WCA measurements of PLLA before laminin functionalization, after EtOH treatment, and after laminin functionalization.
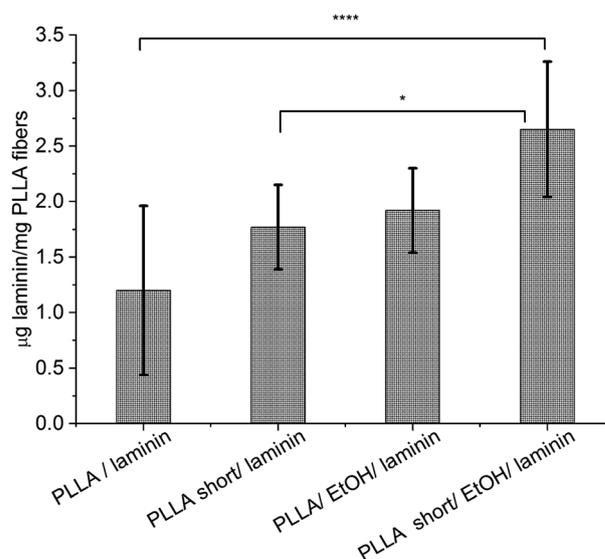

Fig. 3 Quantitative determination of laminin on PLLA fibers *via* BCA assay. Statistical significance: *$p < 0.05$, ****$p < 0.0001$.
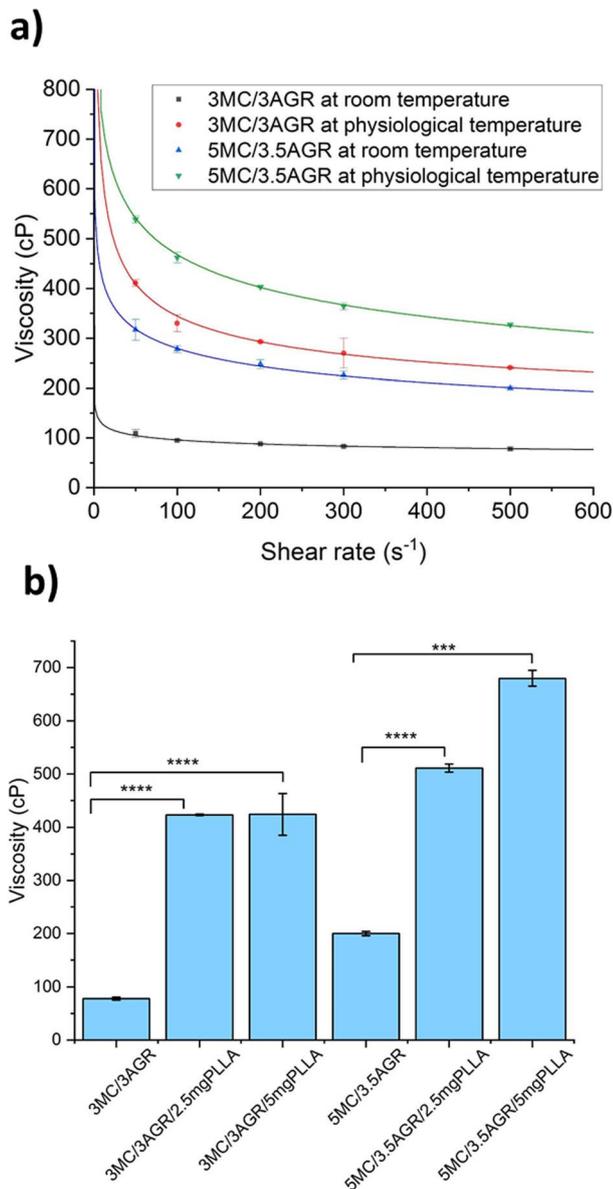
Fig. 4 (a) 3MC/3AGR and 5MC/3.5AGR viscosities *vs.* shear rate fitted with Carreau-model, (b) viscosity of 3MC/3AGR and 5MC/3.5AGR before and after short fibers addition at $\gamma = 500$ s^{-1} at room temperature. Statistical significance: ***$p < 0.001$, ****$p < 0.0001$.

0.94. Irrespective of the temperature, MC/AGR showed the shear-thinning effect, being most pronounced for higher temperature and polymer concentration. The effect of temperature on shear thinning phenomena is well pronounced at lower polymer concentrations (3MC/3AGR) (Fig. 4a).

Another observation is an increase in the viscosity of hydrogel systems with the MC and AGR concentration and the addition of short fibers. The addition of short fibers statistically significantly increased the viscosity of the hydrogel system (Fig. 4b).

3.3.2 Injectability tests. In these studies, injectability measurements are defined as the easiness of hydrogel extrusion

represented as the injection force. According to the literature reports[47,48] there are three components of injection force that were observed during force measurements (Fig. 5b). The first one is a plunger-stopper break-loose force (PBF), which is the force initiating the displacement of the plunger. In our studies, PBF was not analyzed due to using of a special glass syringe with a precisely adjusted plunger, which enables its easy slide resulting in minimization of gliding force under steady conditions, allowing neglecting PBF.[49] The second one is a dynamic glide force (DGF), that provides approximately sustained movement of the hydrogel out of the syringe (Fig. 5b).[50] The last one is a maximum force (F_{max}), the highest force that is needed to move the plunger during the injection (Fig. 5b). Usually, the F_{max} and the PBF are the same values.[51] In our studies, F_{max} results from the materials' nature, *i.e.*, when hydrogel aggregates or accumulation of short fibers reaches the syringe, the force increases rapidly for a moment and then returns to the steady state.

Fig. 6 shows the average forces, *i.e.*, DGF, and F_{max}. The measurements were conducted for a volumetric flow rate of 1 ml min^{-1} (Fig. 6a) and 0.125 ml min^{-1} (Fig. 6b). According to the literature reports, injection ability depends on needle size and geometry, injection rate, *i.e.*, volumetric flow rate, and the viscosity of the hydrogel.[47] In our studies, we used one needle size of 23G as commonly used for manual injection, as it limits invasiveness and increases patients' comfort.[51]

For the applied flow rate of 1 ml min^{-1}, it was observed a statistically significant increase in DGF with hydrogel systems concentrations, and the content of short fibers in the solution (Fig. 6a). Despite the visible trend of increase in F_{max} with increasing viscosity of hydrogel systems, the statistically significant value was observed only between the smallest MC/AGR concentration without PLLA fibers and the highest MC/AGR concentration with the largest amounts of PLLA fibers.

For a flow rate of 0.125 ml min^{-1} (Fig. 6b), the forces were practically independent of the samples' viscosity, and the differences between them were statistically insignificant. For this flow rate, the DGF and F_{max} forces were lower in comparison to 1 ml ml^{-1}.
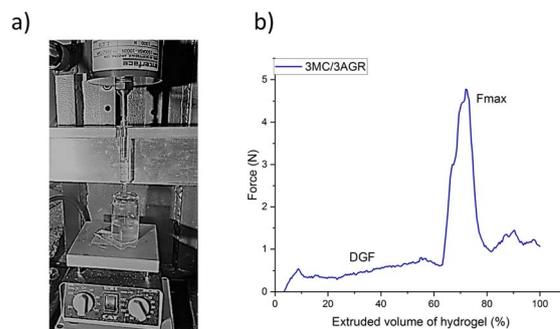

Fig. 5 Injectability test of MC/AGR hydrogels and MC/AGR short PLLA fibers hydrogel systems: (a) digital image of injectability test. The hydrogel system injection into the hydrogel, which simulates storage modulus (G') of the spinal cord, *i.e.* 5–42 kPa,[52] (b) representative example of the force measurement as a function of extruded volume (%) of 3MC/3AGR hydrogel at flow rate 0.125 ml min^{-1}.
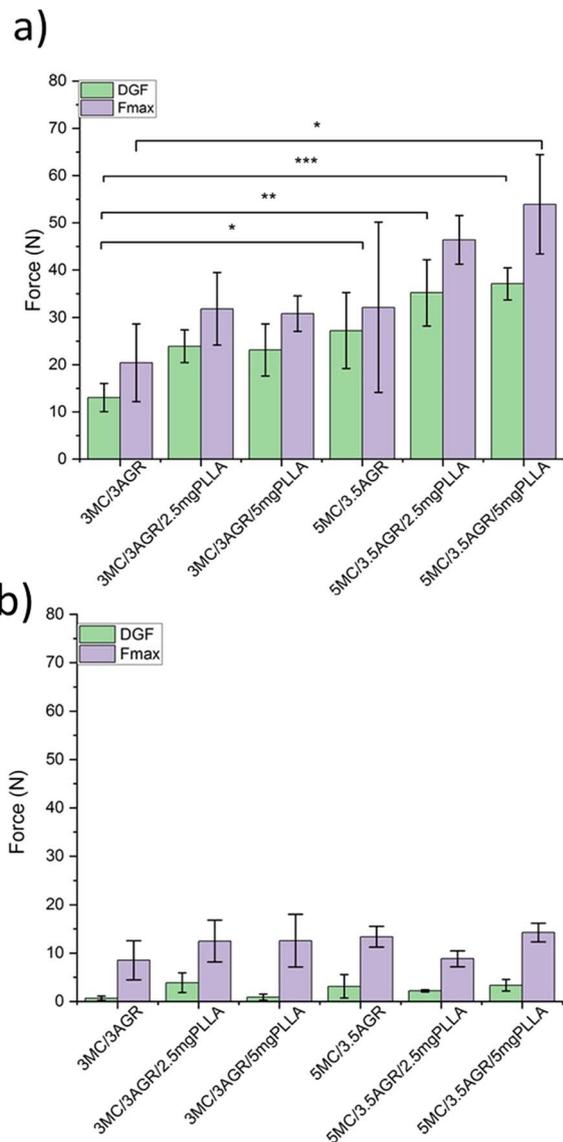
a)

b)

Fig. 6 Average forces, *i.e.*, DGF, and F_{max}, needed to make an injection of hydrogel through a 23G needle for various MC/AGR concentrations and PLLA fibers contents. The applied flow rates of (a) 1 ml min^{-1}, (b) 0.125 ml min^{-1}. Statistical significance: *$p < 0.05$, **$p < 0.01$, ***$p < 0.001$.
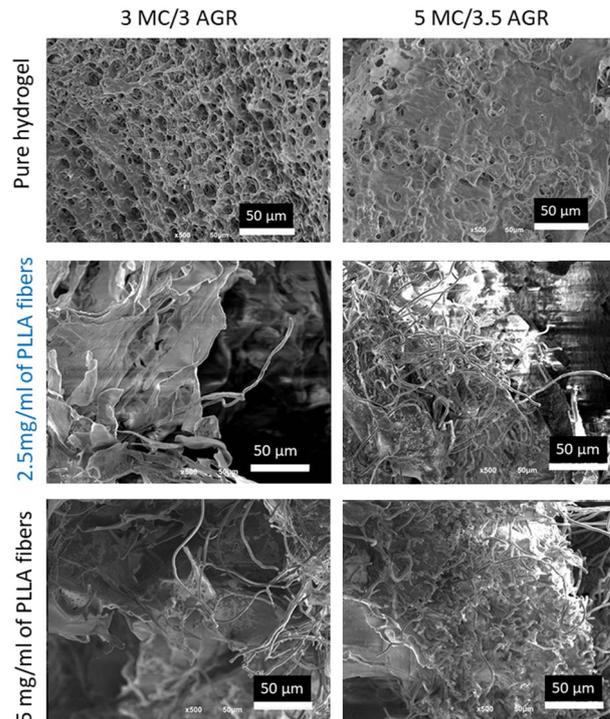

Fig. 7 SEM images of pure 3MC/3AGR and 5MC/3.5AGR hydrogel and after subsequent PLLA short fibers addition.

hydrogel systems extracts after one and three days. Conducting such studies allowed us to assess the materials' relevance for tissue engineering applications.

The results indicated the cell viability was at a similar level as the control (tissue culture plastic (TCP)) and did not show values below 70%. A value of ≥70% under ISO 10993-5 standard is considered to be the limit of nontoxicity. The cell viability of most of the samples was comparable to the control. The exception was the 5MC/3.5AGR_L/F/L sample, where cell
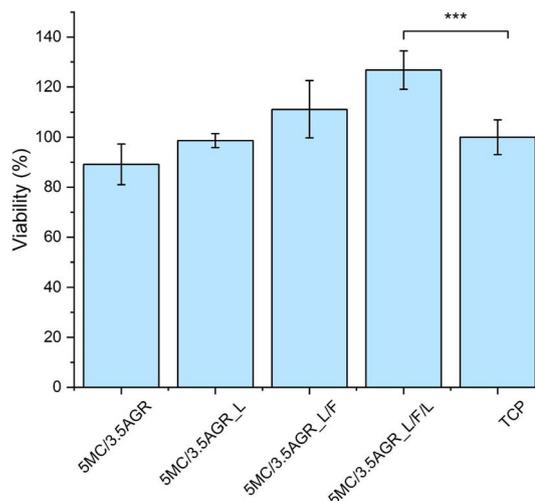
Additionally, for both flow rates, it was observed that short PLA fibers addition increased the F_{max} needed for hydrogel system injection. However, no significant differences in forces with the amounts of added fibers were observed.

3.3.3 SEM. The SEM images presented in Fig. 7 compare the hydrogel of 3MC/3AGR and 5MC/3.5AGR before and after PLLA short fibers addition. The images show the presence of short PLLA fibers inside the hydrogel structure. The morphology of both 3MC/3AGR and 5MC/3.5AGR filled with 2.5 and 5 mg of PLLA short fibers showed complex, 3D characteristic structures.

3.3.4 Biological tests

3.3.4.1 Evaluation of biocompatibility. Viability tests were conducted using Presto Blue assay on the above 5MC/3.5AGR

Fig. 8 Fibroblasts viability tests on extracts. Statistical significance ***$p < 0.001$.

viability was statistically significantly higher in comparison to the control (Fig. 8).

3.3.4.2 Morphology of fibroblasts seeded on hydrogel systems and hydrogel systems loaded with short fibers. The L929 fibroblasts morphology on 5MC/3.5AGR hydrogel, 5MC/3.5AGR_L (hydrogel with added laminin), 5MC/3.5AGR_L/F (hydrogel with added laminin and modified with short PLLA fibers), and 5MC/3.5AGR_L/F/L (hydrogel with added laminin and modified with short PLLA/laminin fibers) using FM are shown in Fig. 9. In comparison to the control TCP (tissue culture plastic) the materials show increased amounts of fibroblasts, their homogeneous distribution on the hydrogel surface. Cellular spreading and extended morphology of cells seeded on hydrogels are characteristic of proper L929 growth and indicator of good material–cell interactions. Such morphology was observed for 5MC/3.5AGR_L and 5MC/3.5AGR_L/F in comparison to the TCP. The 5MC/3.5AGR_L/F/L showed a different distribution than other samples and the control. It could be the effect of cell aggregates and multilayering formation, where cells overgrow on each other forming many layers of variously oriented cells due to a laminin-rich substrate.[53]

A fibroblast morphology is bipolar with parallel orientation to the substrate,[54] such orientation is especially visible on Fig. 9 for hydrogel 5MC/3.5AGR. Cells seeded on 5MC/3.5AGR_L and 5MC/3.5AGR_L/F hydrogels indicated spindle-like morphology characteristic of polar substrates and good cellular interaction. The fibroblast amount on most hydrogels was similar to the control which corresponds with cellular viability (Fig. 8).

3.3.4.3 Morphology of glioma cells seeded on hydrogel systems and hydrogel systems loaded with short fibers. LN18 and WG4 glioma cells cultured on 3D hydrogels substrates: 5MC/3.5AGR,

5MC/3.5AGR_L, 5MC/3.5AGR_L/F, and 5MC/3.5AGR_L/F/L were compared with 2D monolayer culture (TCP). The 2D monolayer culture was characterized by flat cell morphology for both glioma cell lines. The presence of protruded serval broad lamellipodium on 2D monolayer culture was especially visible for both lines after 3 days of culturing (Fig. 10 and 11). The 3D cell culture hydrogels exhibited aggregate formation and related round-shape morphology for LN18 cells after one and three days of cell culture.

Contrary to LN18, the WG4 cells seeded on 3D hydrogels showed spindle morphology with clear polarity after one and three days (Fig. 11).

All hydrogels were noncytotoxic for glioma cell growth and proliferation. The glioma cell from both lines was in various hydrogel heights providing their infiltration in hydrogel volumes.

Images from fluorescence microscopy of WG4 cells cultured on 3D hydrogels substrates were taken in transmitted light axis brightfield mode (TL-BF) and fluorescence mode after 1 and 3 days of culturing. Images in transmission show hydrogels morphology and short fibers occurrence (ESI Fig. B and C,† left column). Cellular skeleton was illustrated in fluorescence mode (ESI Fig. B and C,† middle column). Images from both modes were merged to highlight cellular-hydrogel integration (Fig. Band C,† right column). After 3 days of culturing, WG4
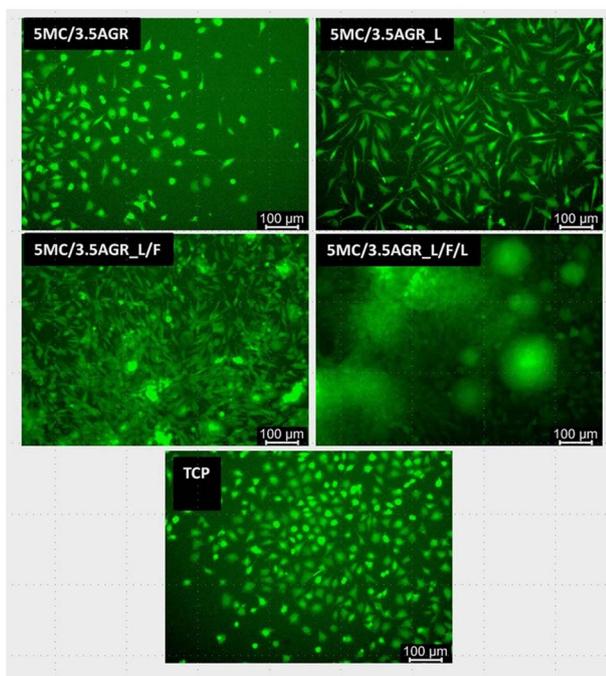

Fig. 9 FM images of L929 fibroblast morphology while seeded on various variants of MC/AGR hydrogel systems after 3 days of culturing.
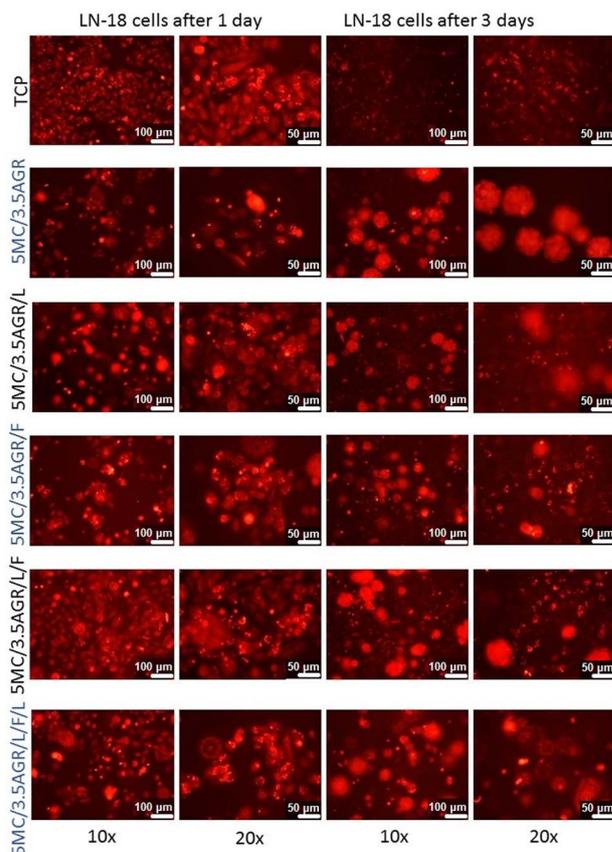

Fig. 10 LN18 glioma cell morphology by FM after 1 and 3 days of culturing.
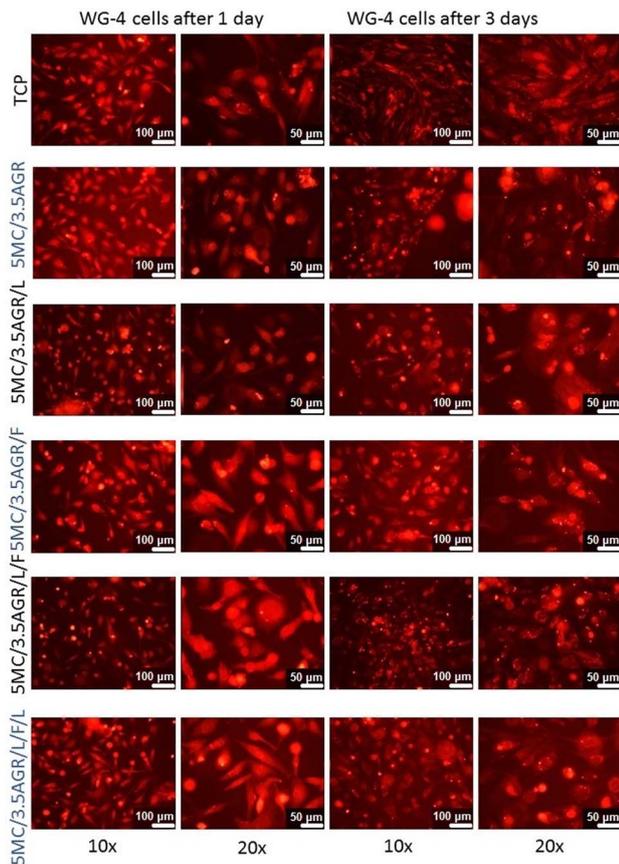
Fig. 11 WG4 glioma cell morphology by FM after 1 and 3 days of culturing.

cells seeded on 5MC/3.5AGR_L/F/L showed the best connection between the cells and show well-developed lamellipodia with filopodia in comparison to other samples and the control.

4. Discussion

In this paper, a thermosensitive injectable MC/AGR hydrogel system loaded with short electrospun bioactive PLLA/laminin fibers as a smart scaffold for tissue engineering or a 3D cell culture model has been studied.

The degradation rate of hydrogel plays an important role in scaffolds implanting and cell-material response. Proper scaffold degradation should provide tissues outgrowth and vascularization at lesion. For instance, scaffolds dedicated bone tissue engineering should not degrade for two weeks, while for central nervous system tissue engineering biomaterial should be stable for *ca.* 1–2 months.[55] In our results, both materials degraded after 18 days indicating, in the future degradation rate should be improved by incorporation of some additives or increasing the concentrations of both hydrogel components. According to the Zhuo et al.,[55] adding polyethylene glycol (PEG) to MC could extend the degradation to ca. 50% after 21 days, and a higher MC contribution in the solution could decrease the degradation rate in hyaluronic acid/MC hydrogel due to its stable chemical structure at physiological conditions.

Still, during our biological studies, both hydrogels weight loss was in the range of 10–17% after 2 days of cell culturing, which according to the literature, *e.g.*, ref. 56 is irrelevant to the 3 day studied cell response.

Laminin, used by us as for modification of short fibers, is ECM native protein that is synthesized after nerve damage and supplies surface cues essential to neurite outgrowth and regeneration.[57] Aliphatic polyesters such as PLLA are biochemically inert, decreasing cell attachment to the material. To overcome this limitation, various chemical (*e.g.* aminolysis, hydrolysis, chemical grafting) and physical (*e.g.* physical adsorption, layer-by-layer assembly) functionalization methods and protein immobilization are used. In comparison to chemical fiber modification methods, the physical adsorption of laminin into PLLA fiber's surface allowed to keep the bulk properties of the polymer and mechanical properties,[43] and simultaneously increase hydrophilicity and provide bioactive surface cues enhancing cell–materials attachment. The studies dedicated to short PLLA fibers modification with laminin and previously treated with EtOH showed the most satisfactory increase of hydrophilicity and laminin attachment. This is most likely the effect of a high surface area of short electrospun fibers, increased surface roughness,[58] and lower surface tension for EtOH-treated mats.[59,60] All of these parameters are favorable from the cellular perspective.

The MC/AGR hydrogel system loaded with short electrospun bioactive PLLA/laminin fibers was characterized in terms of viscosity, injectability, morphology, and biological properties.

The observed increase of viscosity measured at 37 °C is a consequence of the thermal gelation of MC. Regardless of the temperature, the hydrogel system characterized the shear-thinning effect, which is a consequence of molecular disentanglement and chain alignment toward applied forces. It leads to a reduction of molecular interactions and a larger amount of free space, resulting in viscosity reduction. This effect is naturally better manifested in higher molecular weight polymers or in physically crosslinked polymers like our MC/AGR hydrogel at 37 °C, being highly entangled systems. In the case of a relatively low concentration system, for instance, 3MC/3AGR, at room temperature, the entanglement density is expected to be low at rest, so there is no large shear thinning effect. An increase of shear thinning effect for such low concentrated systems is evident at higher temperature at which a physical crosslinking occurs, increasing effective chain entanglements at rest.

Additionally, all of the obtained viscosities of hydrogels and short fibers/hydrogel systems are below 1000 cP (Fig. 4). According to Bradshaw et al.,[61] this value is considered to be a limit of injection ability through a 23 gauge needle. To confirm these reports, additional studies of injectability tests on hydrogels and short fibers/hydrogel systems were carried out.

The injectability tests were conducted to study materials from a practical clinical perspective. Depending on applied injection rates, DGF and F_{max} were different, the higher injection rate resulted in higher DGF and F_{max}. The results were consistent with the literature reports, *i.e.* ref. 50, showing that the slower injection rate could overcome difficulties caused by

large aggregates during hydrogel extrusion, resulting in reduction of injection force.

Our results clearly documented an increase of the F_{max} after short PLLA fibers addition. The lack of any statistically significant differences in forces as a function of added fibers content could be explained by a weak dependence of PLLA fiber orientation along the applied shear on the fibers concentration, at least in this range of concentrations, resulting in insignificant effect on the ultimate viscosity at a particular shear rate.

According to the literature reports *e.g.* Kim *et al.*[40] 30 N is the F_{max}, which is reasonable to make an injection by humans. Above 30 N injection by humans remains difficult or even impossible. From Fig. 6a it is evident that when the flow rate of 1 ml min^{-1} is applied, only 3MC/3AGR, 3MC/3AGR loaded with PLLA fibers, and 5MC/3.5AGR pure hydrogel are within the F_{max} limit. While the flow rate is decreased (Fig. 6b), all of the measured samples showed a F_{max} below 20 N. Thus, similarly to ref. 50, by decreasing the volumetric flow rate, all of the hydrogels could be easily injected through a 23G needle by humans.

The importance of ECM-mimicking morphology provides topographical cues for cellular adhesion and allows nutrients and gas transportation, which is also justified in the literature.[62,63] The morphology of both hydrogel system variants showed unique 3D fibrous structures that, according to literature reports, are similar to native ECM in rat spinal cord.[64,65] Additionally, hydrogel systems functionalized with short PLLA fibers also showed a clear resemblance to porcine native cartilage ECM as shown by Chen *et al.*[66] According to Narkar *et al.*,[67] designed biomaterials for tissue engineering applications should not only mimic native ECM in such biological stimuli as adhesive proteins and provide adequate mechanical properties but also should provide morphology that various cells could respond to.

In vivo increased cell proliferation rates evoked by a favorable environment enhance tissue regeneration faster.[68] Additionally, the laminin-rich scaffolds are especially decent from the perspective of nerve regeneration, where they provide guidance cues to ensuing axons that are capable of migrating from the proximal to distal ends. Such material's functionalization increases their functionalities range: laminin-rich scaffolds not only would enhance nerve regeneration but also, with the use of modern processing methods, could increase bone regeneration capabilities.[69] The presence of a high amount of ECM protein contact guidance cues in the hydrogel system, consistent with literature reports, resulted in increased cell viability.[70]

Another important factor determining scaffold relevance for tissue engineering applications is the morphology of cells subcultured onto the scaffold. Cell morphology is strongly involved in overall physiology and could point out such processes as apoptosis or growth inhibition.[71] Also, cell distribution could provide decent information on whether cells are well attached to the material. The homogenous cell distribution indicates high cell adhesion to the scaffold, while the formation of cellular agglomerated clusters indicates the multilayering formation as a result of laminin-rich substrate. Most of the studied hydrogels substrates showed higher amounts of

flattened and extended cells distributed homogeneously on the surface of the whole material compared to the control. This observation confirmed good physiology and cellular interaction with hydrogels. An unusual morphology of 5MC/3.5AGR_L/F/L (Fig. 9) could be the effect of cellular aggregation or cell multilayering formation, where cells overgrow on each other forming many layers of cells. Since this variant of the hydrogel system had the highest amounts of laminin, the multilayering effect of the cells could be the consequence of intensive ECM production by cells in such an environment and higher proliferation rate, which is clearly visible in Fig. 9. We observed increased viability and proliferation of cells seeded on hydrogels with laminin additive (Fig. 8 and 9), similarly to the literature reports.[72,73]

Glioma cell morphology and motility highly depend on three-dimensional architecture *in vivo*, substrate stiffness, and biochemical signalization.[74,75] It is challenging to provide all of these factors in classic 2D culture. Application of 3D hydrogel model *in vitro* to study glioma cell motility, the morphology, proliferation and function of the cells therein is more adequate to the actual *in vivo* conditions than 2D cultures.

The glioma cell morphology could provide crucial information about their migration pattern, which is a prerequisite for tumor invasiveness and metastasizing ability but also their physiology. A round glioma cell morphology indicates the smallest adherent area with little actin-rich protrusions. Such morphology demonstrates no interactions between the substrate and the cells. Elongated morphology with well-developed filopodia and lamellipodia demonstrates higher migration rates and increased adhesion to the substrate. Additionally, LN18 cells are spindle-shaped and WG4 are more star-shaped cells. Due to the change of the media from standard medium (which contains serums) to stem cell culture medium (without serum, but with growth factors EGF, FGF and supplement B27), both LN18 and WG4 form spheres.[76] Therefore, the spherical shape of the cell seeded on hydrogels may be a sign of the lack of access of cells to the serum in the hydrogel.

Substrate stiffness also is an important parameter in glioma cell proliferation. Pogoda *et al.* reported, glioma cells do not spread on lower stiffness of hydrogel substrates showing round morphology.[75] In other studies, Ulrich *et al.*[77] reported glioma cells seeded on stiffer hydrogel substrates significantly influence motility and increase cellular proliferation in comparison to substrates with mechanical properties similar to native tissues. Glioma cell migration depends on contractile forces generated by actomyosin and relies on the regulation of dynamic spaces between the cellular cytoskeleton and ECM. Stiffer surfaces increase the expression and activity of contractile proteins in glioma cells. Additionally, for glioma cells seeded on the stiffer substrate, the confluency was faster and this phenomenon is most likely the effect of the changed cell cycle upon the change of mechanochemical feedback during mitosis.[77] LN18 cells have a smaller volume than WG4, therefore their interaction with the hydrogel results from the difference in stiffness. We may also cell behavior on our hydrogels according to the Johnson–Kendall–Roberts (JKR) theory which predicts the form of contacts between soft, adhesive surfaces by balancing

adhesion energy, favoring contact, against elastic energy and opposes deformation.[78] When the contact radius of the cell with hydrogel is much larger than solid surface tension/substrate stiffnesses (Ysv/E), the contact is described by the JKR theory, which balances adhesion and elastic stresses. The surface tension contribution is negligible. We presume this to be the case with WG4 on fiber hydrogels. However, when the contact radius is much smaller than Ysv/E, surface tension governs contact mechanics and adhesion mimics adsorption on a fluid interface. The undeformed solid surface hits the particle at a fixed contact angle given by the generalized Young's law. Elastic forces are negligible. This behavior is observed for LN18 cells on hydrogels with lower Young's modulus. It corresponds also with previous observation, that LN18 which are smaller than WG4, seeded collapse in hydrogels with lower Young modulus as spheres. The retention of the spherical shape is additionally caused by lower access to the serum in media.[76]

Additionally, biochemical cues play a crucial role in glioma cells' stimulation or inhibition. According to the literature,[79] laminin stimulates human glioma cell migration *in vitro*. Thus, in our studies, the WG4 cell showed the spindle-like morphology and the best-developed lamellipodia with filopodia, accompanied cellular migration, while seeded on the sample with the highest amounts of laminin. Future studies could use such a 3D laminin-rich hydrogel platform loaded with fibers to investigate the characteristic features of glioma cells and could be an essential part of the complex dependencies of growth factors, integrins, and extracellular matrix during glioma cell invasion.

Conclusions

The conducted research was focused on designing modern and smart kinds of material – injectable thermosensitive hydrogel loaded with short bioactive electrospun nanofibers. Although hydrogels and electrospun fibers separately are commonly used in tissue engineering, combination of short electrospun PLLA/laminin fibers with MC/AGR hydrogel is a novelty in the context of currently published literature reports. The obtained results provide fundamental knowledge of composite material which could be valuable for both materials science and tissue engineering. Our results show that laminin incorporation *via* physical adsorption to the PLLA short fibers with previous EtOH treatment efficiently decreased the water contact angle. The properties of PLLA short fibers, *i.e.*, a large surface area, and roughness, as well as adequate sample preparation using EtOH reducing surface tension, lead to the incorporation of the largest amount of protein. The introduction of modified short fibers into hydrogel allows the system to mimic the native ECM morphology, providing good cellular response, *i.e.*, cell–material interactions and increased fibroblasts and WG4 cell proliferation.

Despite the fact that addition of short fibers lead to increase of hydrogel system viscosity, injectability tests have shown that, depending on the injection rate used, hydrogels loaded with short fibers could be extruded with a force considered reasonable for a human.

In the future studies, thermosensitive hydrogels loaded with short fibers could be additionally modified with some additives such as PEG to improve the hydrogels degradation rate, and studied more thoroughly in terms of neural cell response. On the other hand, considering increased stiffness of material, its injection ability and lack of effective therapies for cartilage defects, cartilage tissue engineering could be also the right direction.

On the other hand, considering good glioma cells response, such approaches should serve as a 3D cell culturing platform for studying, understanding and manipulating glioma cell physiology. An interesting study for the future assumes hydrogel systems that could be integrated with microfluidic devices to study static and dynamic glioma cell growth conditions as more sophisticated model for the study of glioma cells behavior in a controlled microenvironment generated by fluidic conditions in an ECM-biomimetic hydrogel matrix.

Author contributions

B. N. S., D. K. and P. S. conceived the project. B. N. S. optimized and developed the hydrogel systems loaded with short bioactive fibers. B. N. S. performed WCA, BCA, viscosity measurements and analysed the results, B. N. S. and G. M. performed injectability tests. D. K. performed *in vitro* tests on fibroblasts. B. N. S. and D. K. analysed *in vitro* studies and performed morphological observations of fibroblasts, I. A. C. performed *in vitro* tests on glioma cells, analysed and performed morphological observations. B. N. S, D. K., G. M., I. A. C. and P. S. wrote the manuscript. B. N. S. providedfinancial support.

Conflicts of interest

There are no conflicts to declare.

Acknowledgements

References

1 Y. Zhao, H. Mu, Y. Huang, S. Li, Y. Wang, R. A. Stetler and Y. Shi, *J. Neuroinflammation*, 2022, **19**(1), 1–19.

2 A. Movahedpour, O. Vakili, M. Khalifeh, P. Mousavi, A. Mahmoodzadeh, M. Taheri-Anganeh and S. H. Khatami, *Cell Biochem. Funct.*, 2022, **40**(3), 232–247.

3 V. Strøm, G. Månum, M. Arora, C. Joseph, A. Kyriakides, M. Le Fort and J. Middleton, *J. Rehabil. Med.*, 2022, **54**, jrm00302.

4 D. Clark, J. B. Cheserem, I. D. Bhagavatula, A. Figaji and P. Hutchinson, *Neurosurgery and Global Health*, Springer, Cham, 2022, pp. 19–32.

5 A. P. Patel, J. L Fisher, E. Nichols, F. Abd-Allah, J. Abdela, A. Abdelalim and C. Fitzmaurice, *Lancet Neurol.*, 2019, **18**(4), 376–393.

6 O. Rominiyi and S. J. Collis, *Mol. Oncol.*, 2022, **16**(1), 11–41.

7 B. Ucar, *Neurochem. Int.*, 2021, **146**, 105033.

8 D. Silva, R. A. Sousa and A. J. Salgado, *Mater. Today Bio*, 2021, **9**, 100093.

9 C. T. Lu, Y. Z. Zhao, H. L. Wong, J. Cai, L. Peng and X. Q. Tian, *Int. J. Nanomed.*, 2014, **9**, 2241.

10 Q. Li, X. Shao, X. Dai, Q. Guo, B. Yuan, Y. Liu and W. Jiang, *NPG Asia Mater.*, 2022, **14**(1), 1–14.

11 M. Jury, I. Matthiesen, F. Rasti Boroojeni, S. L. Ludwig, L. Civitelli, T. E. Winkler and D. Aili, *Adv. Healthcare Mater.*, 2022, **11**(11), 2102097.

12 N. Shah, P. M. Hallur, R. A. Ganesh, P. Sonpatki, D. Naik, K. P. Chandrachari and A. Chaubey, *Sci. Rep.*, 2021, **11**(1), 1–18.

13 E. Ansorena, P. De Berdt, B. Ucakar, T. Simón-Yarza, D. Jacobs, O. Schakman and A. des Rieux, *Int. J. Pharm.*, 2013, **455**(1–2), 148–158.

14 A. Hsieh, T. Zahir, Y. Lapitsky, B. Amsden, W. Wan and M. S. Shoichet, *Soft Matter*, 2010, **6**, 2227–2237.

15 D. Wu, E. S. Pak, C. J. Wingard and A. K. Murashov, *Neurosci. Lett.*, 2012, **507**(1), 72–77.

16 A. Lis, D. Szarek and J. Laska, *Polim. Med.*, 2013, **43**(4), 302–312.

17 F. Guilak, D. M. Cohen, B. T. Estes, J. M. Gimble and W. Liedtke, *Cell Stem Cell*, 2009, **5**(1), 17–26.

18 C. J. Rivet, K. Zhou, R. J. Gilbert, D. I. Finkelstein and J. S. Forsythe, *Biomatter*, 2015, **5**(1), e1005527.

19 K. S. Anseth, C. N. Bowman and L. Brannon-Peppas, *Biomaterials*, 1996, **17**(17), 1647–1657.

20 J. R. Thonhoff, D. I. Lou, P. M. Jordan, X. Zhao and P. Wu, *Brain Res.*, 2008, **1187**, 42–51.

21 J. George, C. C. Hsu, L. T. B. Nguyen, H. Ye and Z. Cui, *Biotechnol. Adv.*, 2020, **42**, 107370.

22 Y. A. Miroshnikova, J. K. Mouw, J. M. Barnes, M. W. Pickup, J. N. Lakins, Y. Kim and V. M. Weaver, *Nat. Cell Biol.*, 2016, **18**(12), 1336–1345.

23 B. Niemczyk-Soczynska, A. Zaszczynska, K. Zabielski and P. Sajkiewicz, *Materials*, 2021, **14**(22), 6899.

24 L. Buzanska, M. Zychowicz, A. Sarnowska and K. Domanska-Janik, *Postepy Biochem.*, 2013, **59**(2), 175–186.

25 Y. T. Wei, W. M. Tian, X. Yu, F. Z. Cui, S. P. Hou, Q. Y. Xu and I. S. Lee, *Biomed. Mater.*, 2007, **2**(3), S142.

26 N. Comolli, B. Neuhuber, I. Fischer and A. Lowman, *Acta Biomater.*, 2009, **5**(4), 1046–1055.

27 F. Ordikhani, S. Sheth and S. P. Zustiak, *Int. J. Pharm.*, 2017, **516**(1–2), 71–81.

28 T. Ozeki, D. Kaneko, K. Hashizawa, Y. Imai, T. Tagami and H. Okada, *Int. J. Pharm.*, 2012, **427**(2), 299–304.

29 R. Curvello, V. Kast, M. H. Abuwarwar, A. L. Fletcher, G. Garnier and D. Loessner, *Front. digit. health*, 2021, **3**, 704584.

30 B. Niemczyk-Soczynska, P. Sajkiewicz and A. Gradys, *Polymers*, 2022, **14**(9), 1810.

31 B. Niemczyk-Soczynska, A. Gradys, D. Kolbuk, A. Krzton-Maziopa and P. Sajkiewicz, *Polymers*, 2019, **11**(11), 1772.

32 B. Niemczyk-Soczynska, A. Gradys, D. Kolbuk, A. Krzton-Maziopa, P. Rogujski, L. Stanaszek, B. Lukomska and P. Sajkiewicz, *RSC Adv.*, 2022, **12**(41), 26882–26894.

33 B. Niemczyk-Soczynska, J. Dulnik, O. Jeznach, D. Kolbuk and P. Sajkiewicz, *Micron*, 2021, **145**, 103066.

34 M. Wang, J. Du, M. Li, F. Pierini, X. Li, J. Yu and B. Ding, *Biomater. Sci.*, 2023, 1–12.

35 K. Zhang, H. Zheng, S. Liang and C. Gao, *Acta Biomater.*, 2016, **37**, 131–142.

36 H. S. Koh, T. Yong, C. K. Chan and S. Ramakrishna, *Biomaterials*, 2008, **29**(26), 3574–3582.

37 R. Milner, M. Wilby, S. Nishimura, K. Boylen, G. Edwards, J. Fawcett and R. Pytela, *Dev. Biol.*, 1997, **185**(2), 215–228.

38 E. J. Falde, J. Wang and M. W. Grinstaff, *RSC Adv.*, 2017, **7**(78), 49795–49798.

39 T. Bodnar, A. Sequeira and M. Prosi, *Appl. Math. Comput.*, 2011, **217**(11), 5055–5067.

40 M. H. Kim, B. S. Kim, H. Park, J. Lee and W. H. Park, *Int. J. Biol. Macromol.*, 2018, **109**, 57–64.

41 J. Dulnik, D. Kolbuk, P. Denis and P. Sajkiewicz, *Eur. Polym. J.*, 2018, **104**, 147–156.

42 I. A. Ciechomska, P. Przanowski, J. Jackl, B. Wojtas and B. Kaminska, *Sci. Rep.*, 2016, **6**(1), 1–15.

43 B. Niemczyk-Soczynska, A. Gradys and P. Sajkiewicz, *Polymers*, 2020, **12**(11), 2636.

44 D. Kolbuk, M. Ciechomska, O. Jeznach and P. Sajkiewicz, *RSC Adv.*, 2022, **12**(7), 4016–4028.

45 L. He, S. Tang, M. P. Prabhakaran, S. Liao, L. Tian, Y. Zhang and S. Ramakrishna, *Macromol. Biosci.*, 2013, **13**(11), 1601–1609.

46 S. Kakinoki and T. Yamaoka, *J. Mater. Chem. B*, 2014, **2**(31), 5061–5067.

47 F. Cilurzo, F. Selmin, P. Minghetti, M. Adami, E. Bertoni, S. Lauria and L. Montanari, *AAPS PharmSciTech*, 2016, **17**(6), 1508.

48 Q. Zhang, M. A. Fassihi and R. Fassihi, *AAPS PharmSciTech*, 2018, **19**(4), 1520–1528.

49 K. Yoshino, K. Nakamura, A. Yamashita, Y. Abe, K. Iwasaki, Y. Kanazawa and S. Suzuki, *J. Pharmaceut. Sci.*, 2014, **103**(5), 1520–1528.

50 A. Ryl and P. Owczarz, *Polymers*, 2020, **12**(10), 2260.

51 A. Shavandi, A. E. D. A. Bekhit, Z. Sun and M. A. Ali, *J. Sol. Gel Sci. Technol.*, 2016, **77**(3), 675–687.

52 R. D. Bartlett, D. Choi and J. B. Phillips, *Regen. Med.*, 2016, **11**(7), 659–673.

53 T. Boontheekul, H. J. Kong and D. J. Mooney, *Biomaterials*, 2005, **26**(15), 2455–2465.

54 N. Lakshman, A. Kim and W. M. Petroll, *Exp. Eye Res.*, 2010, **90**, 350–359.

55 F. Zhuo, X. Liu, Q. Gao, Y. Wang, K. Hu and Q. Cai, *Mater. Sci. Eng. C*, 2017, **81**, 1–7.

56 Y. Wu, Z. Yang, J. B. K. Law, A. Y. He, A. A. Abbas, V. Denslin and E. H. Lee, *Tissue Eng.*, 2017, **23**(1–2), 43–54.

57 D. McDonald, C. Cheng, Y. Chen and D. Zochodne, *Neuron Glia Biol.*, 2006, **2**, 139.

58 Y. Ren, S. Wang, R. Liu, J. Dai, X. Liu and J. Yu, *RSC Adv.*, 2016, **6**(36), 30139–30147.

59 M. Gryta, *Chem. Pap.*, 2013, **67**(9), 1201–1209.

60 C. Zhang, X. Yuan, L. Wu, Y. Han and J. Sheng, *Eur. Polym. J.*, 2005, **41**(3), 423–432.

61 J. Bradshaw and S. White, *ONdrugDelivery*, 2018, **91**, 16–21.

62 G. S. Hussey, J. L. Dziki and S. F. Badylak, *Nat. Rev. Mater.*, 2018, **3**(7), 159–173.

63 R. T. Miller, *Matrix Biol.*, 2017, **57**, 366–373.

64 A. Padhi and A. S. Nain, *Ann. Biomed. Eng.*, 2020, **48**(3), 1071–1089.

65 D. X. Ban, Y. Liu, T. W. Cao and S. J. Gao, *Spinal Cord*, 2017, **55**(4), 411–418.

66 Y. C. Chen, R. N. Chen, H. J. Jhan, D. Z. Liu, H. O. Ho, Y. Mao and M. T. Sheu, *Tissue Eng. C Methods*, 2015, **21**(9), 971–986.

67 A. R. Narkar, Z. Tong, P. Soman and J. H. Henderson, *Biomaterials*, 2022, **283**, 121450.

68 A. B. Bloom and M. H. Zaman, *Physiol. Genom.*, 2014, **46**(9), 309–314.

69 S. Ozkan, D. M. Kalyon and X. Yu, *J. Biomed. Mater. Res., Part A*, 2010, **92**(3), 1007–1018.

70 R. Junka, C. M. Valmikinathan, D. M. Kalyon and X. Yu, *J. Biomim. Biomater. Tissue Eng.*, 2013, **3**(4), 494–502.

71 B. Sarker, R. Singh, R. Silva, J. A. Roether, J. Kaschta, R. Detsch and A. R. Boccaccini, *PLoS One*, 2014, **9**(9), e107952.

72 R. Jain and S. Roy, *ACS Biomater. Sci. Eng.*, 2020, **6**(5), 2832–2846.

73 Y. Long, L. Yan, H. Dai, D. Yang, X. Wu, X. Dong and Y. Chen, *Mater. Sci. Eng. C*, 2020, **116**, 111258.

74 Y. Huang, L. Tong, L. Yi, C. Zhang, L. Hai, T. Li and X. Yang, *Mol. Med. Rep.*, 2018, **17**(1), 250–256.

75 K. Pogoda, R. Bucki, F. J. Byfield, K. Cruz, T. Lee, C. Marcinkiewicz and P. A. Janmey, *Biomacromolecules*, 2017, **18**(10), 3040–3051.

76 X. Hong, K. Chedid and S. N. Kalkanis, *Int. J. Oncol.*, 2012, **41**(5), 1693–1700.

77 T. A. Ulrich, E. M. de Juan Pardo and S. Kumar, *Cancer Res.*, 2009, **69**(10), 4167–4174.

78 R. W. Style, C. Hyland, R. Boltyanskiy, J. S. Wettlaufer and E. R. Dufresne, *Nat. Commun.*, 2013, **4**(1), 1–6.

79 B. B. Tysnes, H. K. Haugland and R. Bjerkvig, *Invasion Metastasis*, 1997, **17**(5), 270–280.